Journal of Materials Chemistry A

Accepted Manuscript

ROYAL SOCIETY OF CHEMISTRY

www.rsc.org/materialsA

Journal Name

ARTICLE

Efficient hollow double-shell photocatalysts for the degradation of organic pollutants under visible light and in darkness

Received 00th January 20xx,
Accepted 00th January 20xx

DOI: 10.1039/x0xx00000x

www.rsc.org/

Chinh- Chien Nguyen, Nhu- Nang Vu and Trong- On Do*

The development of efficient photocatalysts that can work both under visible light and in darkness remains an important research target for environmental applications. A large number of photocatalysts have been reported, but they still suffer from low activity that originates from fundamental efficiency bottlenecks: i.e.., weak photon absorption and poor electron–hole pair separation when operating under irradiation, and poor electron storage capacity when operating in darkness. Herein, we report the first synthesis of hollow double-shell H:Pt-WO_3/TiO_2-Au nanospheres with high specific surface area, large TiO_2/WO_3 interfacial contact and strong visible light absorption. Because of these features, this type of nanocomposite shows high charge separation and electron storage capacity, and exhibits efficient degradation of organic pollutants both under visible light (λ ≥ 420 nm) and in darkness. In addition, CO_2 generation from formaldehyde gave a high quantum efficiency of 77.6%.

Introduction

Semiconductor-based photocatalysts are attractive candidates for clean energy production and for environmental applications, such as air purification and wastewater treatment. TiO_2, one of the more widely used semiconducting metal oxides, has received enormous research interest in the past few decades, due to its exceptional ability to decompose organic pollutants, as well as its corrosion resistance, durability, nontoxicity, and low cost.[1, 2] Unfortunately, the application of TiO_2 is limited to UV light, which makes up only ~4% of the energy of incident solar spectrum.[3,4] To overcome this limitation, research efforts have been focused on the development of photocatalysts with strong visible-light absorption, which accounts for 43% of the energy of the solar spectrum. However, the developed materials still suffer from two fundamental drawbacks: weak photon absorption and poor electron–hole pair separation.[5]

To overcome the drawbacks of photocatalysts that only function under light illumination, the development of a photocatalytic system that can work both under light irradiation and in darkness is urgently required. The underlying concept is the coupling of a semiconductor (as an electron generator) with another substance (as an electron acceptor), wherein the semiconductor provides photo-excited electrons under light irradiation and the coupled substance receives and stores the electrons; the stored electrons are subsequently released in darkness for organic pollutant decomposition.[6] Despite several reports by Fujishima et al. relating to a photocatalyst based on the WO_3/TiO_2 heterostructure, few systems exhibiting the desired functionality have been reported.[7-10] As seen in **Scheme SI-1**, due to the matching band energy levels, excited electrons from the conduction band of TiO_2 can be transferred to that of WO_3, wherein the electrons could be stored for reaction in darkness.[6, 8-10] It should be noted that the minimal WO_3/TiO_2 heterostructure interface prepared by conventional methods restricts both charge separation and electron storage capacity. Also, this system absorbs only UV light, meaning its photocatalytic activity under visible light and electron charge–discharge behaviour were both poor. Therefore, to use solar energy more efficiently, photocatalysts that absorb the entire solar spectrum and possess high electron storage ability must be developed.

The use of plasmonic nanoparticles (NPs) and surface modification are the main methods that have been proposed to achieve this enhancement.[11,12] Au, Ag, and Cu NPs can harvest visible light through surface plasmon resonance (SPR) to produce “hot” electrons on their surfaces.[13] These “hot” electrons can transfer to the neighbouring semiconductor for participation in chemical reactions via an interface, thereby enhancing catalyst efficiency.[14,15] Of these metal NPs, Au NPs most strongly absorb visible light and efficiently catalyse the decomposition of organic pollutants.[16] In addition, surface modification through hydrogen treatment to introduce oxygen vacancies can create impurity states in forbidden areas of the band structure, leading to improved photoabsorption and electron storage. Hence, this strategy provides an efficient route to the development of functional materials.[17]

Nanocomposite-based hollow structure photocatalysts have recently attracted much research attention because of their unique properties, *viz.* their nanoscale wall thickness, large interface between components, which plays a critical role in

Department of Chemical Engineering, Laval University, Quebec, G1V 0A8, Canada
Email: trong-on.do@gch.ulaval.ca; Fax +1-418-656-5993; Tel.: +1-418-656-3774

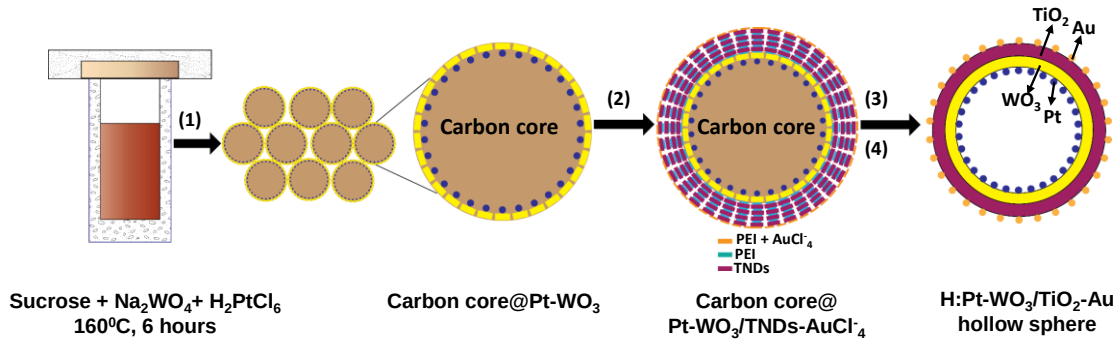

Figure 1. Schematic illustration for the synthesis of hollow double-shell H:Pt-WO_3/TiO_2-Au nanospheres: 1) one-pot synthesis of Pt-WO_3@carbon colloidal spheres, 2) coating with TNDs using a layer-by-layer strategy followed by Au precursor loading, 3) calcination at 550 °C for 3 h, and 4) hydrogen treatment at 350 °C for 1 h.

photogenerated charge transfer, and high porosity within the walls, which reduces the diffusion length and improves the accessibility of active sites for the reactants.[18, 19] Additionally, multiple reflections within the hollow cavity enhance the efficient use of the light source, leading to the production of more photogenerated charge carriers.[20]

In this study, we developed a new type of hollow double-shell photocatalyst based on our recently developed approach.[21-22] This new type of hollow photocatalyst consists of two components: (i) an electron storage material (Pt-WO_3) and (ii) an electron generator (TiO_2-Au); herein, hollow double-shells are formed and two metal NPs (Pt as a co-catalyst and Au as strong visible-light SPR absorber) are selectively loaded onto WO_3 and TiO_2, respectively. This material is then treated with hydrogen to enlarge its light absorption spectrum and to create trapping sites that allow electron storage. This type of hollow double-shell nanocomposite has unique properties, such as high specific surface area, large TiO_2/WO_3 interfacial contact, strong sunlight absorption, high electron–hole separation, and large electron storage capacity. As a result, the prepared material showed excellent activity for the degradation of formaldehyde (HCHO), a major indoor air pollutant, under visible light and in darkness.

Results and discussion

The production of this photocatalyst begins with the one-pot synthesis of Pt-WO_3/carbon core-shell nanospheres, which are subsequently coated with titanate nanodisk (TND) titania precursors using a layer-by-layer technique employing poly(ethyleneimine) (PEI) as a polyelectrolyte.[18,23] Due to the negatively charged surface of carbonaceous nanospheres (carbon core), the positively charged PEI easily binds to the carbon core via electrostatic forces, and converts into a positively charged core surface.[19, 24, 25] Subsequently, negatively charged TNDs are adsorbed. The layer-by-layer technique combined with the uniform size of TNDs allows the tuning of shell thickness. The Au precursor ($AuCl^-_4$) is then loaded on carbon core@Pt-WO_3/TNDs to produce carbon core@Pt-WO_3/TNDs-$AuCl^-_4$ (see the experimental section in SI for details). In the second step, the carbon cores and other organic compounds are removed from the obtained core-shell nanospheres by calcination in air to form hollow Pt-WO_3/TiO_2-Au nanospheres (namely Pt-WO_3/TiO_2-Au), which then undergo H_2 treatment to afford the H_2-treated hollow double-shell Pt-WO_3/TiO_2-Au nanospheres (denoted as H: Pt-WO_3/TiO_2-Au), as depicted in **Figure. 1** and **Scheme SI2.**

It is worth noting that the calcination step in the synthesis is significant, as it generates microporosity in the shells by removing the carbon core and PEI. This microporosity promotes hydrogen contact with the TiO_2 and WO_3 surfaces and thereby lowers the required H_2 treatment temperature. In this way, high specific surface area, large TiO_2/WO_3 interface, strong visible light absorption, effective charge separation, and high electron storage capacity can be achieved. To the best of our knowledge, this is the first synthesis of this type of hollow double-shell H_2-treated WO_3/TiO_2 nanocomposite based on carbon colloidal spheres combined with the layer-by-layer technique.

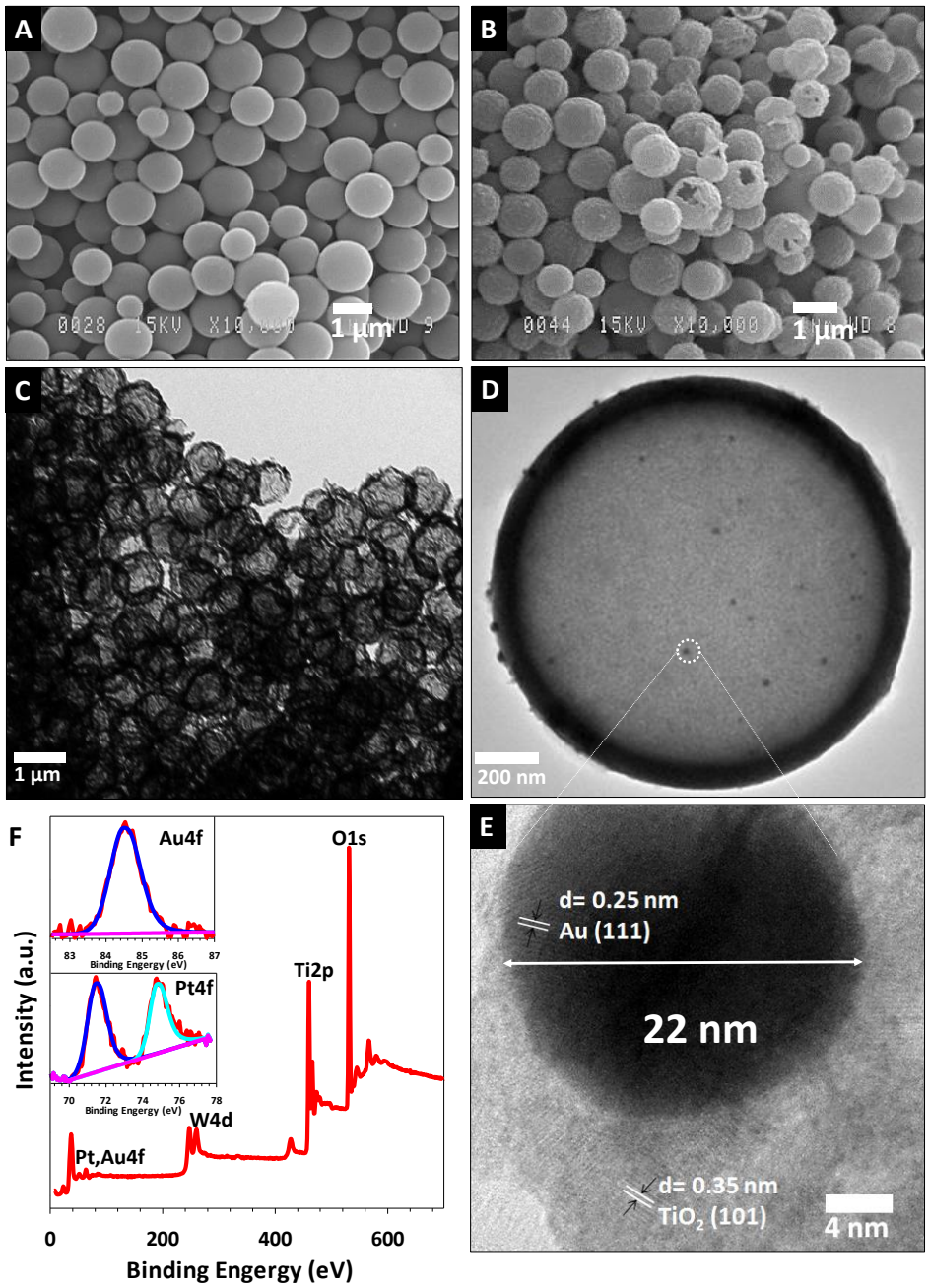

Figure 2. A, B) SEM images of Pt-WO_3/TiO_2-Au before and after calcination followed by hydrogen treatment; C, D) TEM image of the hollow H:Pt-WO_3/TiO_2-Au**; E)** High resolution TEM image of hollow H:Pt-WO_3/TiO_2-Au; F) Survey spectrum of hollow H:Pt-WO_3/TiO_2-Au, inset XPS of Au and Pt**.**

Figure 2A,B shows scanning electron microscopy (SEM) images of the Pt-WO_3/TiO_2-Au core-shell sample before (A) and after calcination and subsequent H_2 treatment (B). The nanospheres are quite uniform, with an average diameter of 1 µm. A slight change in morphology is observed before the carbon colloidal core is removed and after hydrogen treatment. As seen in **Figure 2B**, some broken particles clearly indicate the presence of the hollow nanospheres. These might be formed during calcination for carbon core removal. The presence of these holes, in fact, should be beneficial for photocatalysis as they enhance the diffusion of reactants and light through the shell of the hollow spheres (*vide infra*).[26,27] The morphology of the hollow H:Pt-WO_3/TiO_2-Au sample was further characterized by transmission electron microscopy (TEM) (**Figure 2C, D**). Hollow spheres of ~1 µm in average diameter were observed (**Figure 2C**). Moreover, Au NPs with an average size of 22 nm are evenly distributed on the wall surface of the TiO_2 HNSs (**Figure 2D**) while Pt NPs are not observed, probably due to the Pt particles being small and highly dispersed in the hollow nanocomposite. The thickness of the HNS shell is estimated to be around 80 nm. The high-resolution TEM image (**Figure 2E**) shows the lattice fringes of both TiO_2 and Au, thus indicating the highly crystalline nature of TiO_2 and the Au NPs. The lattice fringe with a d-spacing of 0.35 nm can be assigned to the (101)

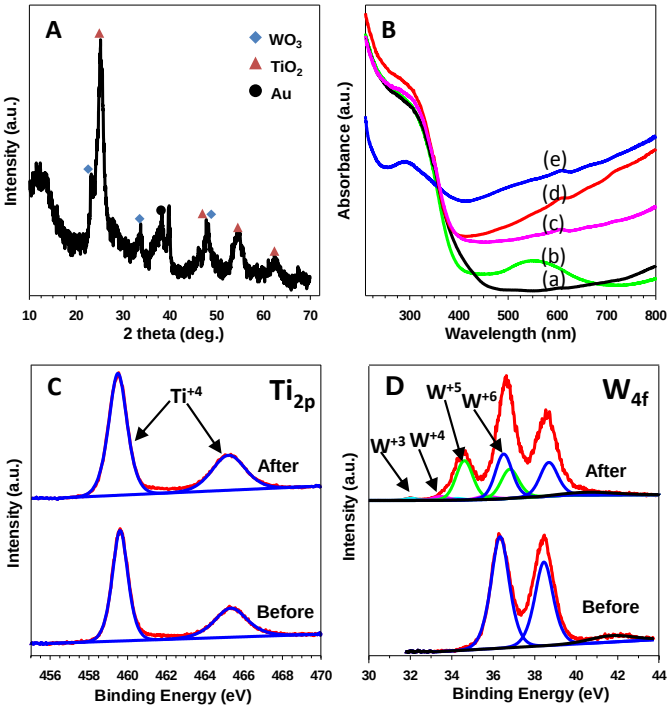

Figure 3. **A:** Powder XRD spectrum of hollow H:Pt-WO_3/TiO_2-Au; **B:** UV-vis spectra of different samples: (a) hollow Pt-WO_3/TiO_2, (b) hollow Pt-WO_3/TiO_2-Au before H_2 treatment; (c) hollow H:Pt-WO_3/TiO_2, (d) hollow H:Pt-WO_3/TiO_2-Au, and (e) hollow H:Pt-WO_3 after hydrogen treatment; **C, D:** XPS Ti 2p and W 4f spectra of Pt-WO_3/TiO_2-Au before and after H_2 treatment.

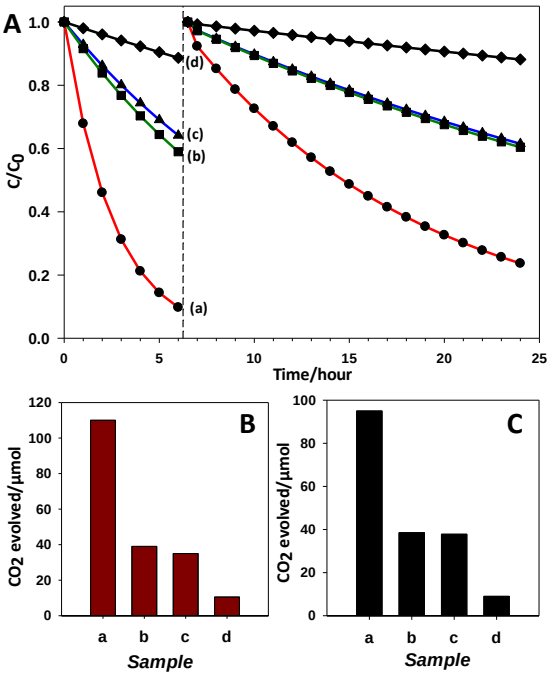

Figure 4. A) Degradation of HCHO as a function of reaction time under visible light illumination (λ≥420 nm) and in the dark; B,C) Amount of CO_2 generated over 6 h in visible light and 18 h in the dark; (a) hollow H:Pt-WO3/TiO2-Au; (b) hollow H:Pt-WO3/TiO2; (c) hollow H:Pt-WO3; (d) conventional H:Pt -WO3 (prepared from commercial WO3 powders). Reaction conditions: catalysts: 50 mg; irradiated area: 4 cm^2. Light source: simulated solar light 300W Xe lamp with 420 nm cut-off filter.

lattice plane of anatase TiO_2, and the fringe with a d-spacing of 0.25 nm belongs to the (111) lattice plane of Au with a face-centred cubic phase.[28] **Fig. 2E** also shows intimate contact between Au and TiO_2. This close contact between the metal and the semiconductor may enhance charge transfer between them, and consequently the photocatalytic efficiency.[29, 30] As seen in **Figure SI-1**, significant shrinking of the hollow area of H:Pt-WO_3 (~500nm in size) without coated TNDs was observed. Therefore, it should be noted that the coated TNDs play the critical role of maintaining the spherical shape after calcination and hydrogen treatment. **Figure 2F** shows the X-ray photoelectron spectroscopy (XPS) spectrum of the hollow H:Pt-WO_3/TiO_2-Au spheres. The photoelectron peaks for Ti2p and W4d appear clearly at binding energies of 460 and 248 eV, respectively. As seen in the inset of **Figure 2F**, the Pt XPS spectra show two peaks at 71.41 and 74.76 eV attributed to metallic Pt, confirming the presence of Pt in the sample, while the Au 4f XPS spectra exhibit a peak at 84.4 eV characteristic of Au^0 on TiO_2.[31] Elemental analysis by inductively coupled plasma mass spectrometry (ICP-MS) reveals that the Au and Pt loadings are 3.0 and 2.5 wt%, respectively. The H:Pt-WO_3/TiO_2-Au sample was also analysed by energy-dispersive spectroscopy (EDS), as shown in **Figure SI 2**. The EDS spectra clearly show that W and Ti are the main constituent elements and that the atomic W:Ti ratio is around 1:1 in the nanocomposite.

The X-ray diffraction pattern of the hollow double-shell H:Pt-WO_3/TiO_2-Au sample is shown in **Figure 3A**, indicating the presence of WO_3, TiO_2, and Au in the material; no XRD peak characteristic of Pt was detected. As mentioned above, this could be due to the small size of the Pt NPs (< 5 nm). The WO_3 phase is confirmed by the peak at 2θ = 23°. The peak at 2θ = 25.2° matches well with the anatase phase of TiO_2,[32] while the peak at 38.5° corresponds to the (111) plane of Au.[33] Meanwhile, the intensities of the WO_3 and TiO_2 phases in the XRD patterns are relatively weak because of the NP size and the increase in the WO_3/TiO_2 interface in the nanocomposite.[34-36] **Figure 3B** shows the UV-vis absorption spectra of different calcined hollow samples before and after H_2 treatment: hollow Pt-WO_3/TiO_2 in the absence of Au, Pt-WO_3/TiO_2-Au (both before H_2 treatment), hollow H:Pt-WO_3, hollow H:Pt-WO_3/TiO_2, and hollow H:Pt-WO_3/TiO_2-Au (after H_2 treatment). For the samples untreated with H_2 (**Fig. 3B-a,b**), the UV-vis spectra are mostly identical, except for a peak centred at 550 nm that is attributed to the SPR of Au NPs in the Pt-WO_3/TiO_2-Au sample.[14] Interestingly, after H_2 treatment, all the samples show strong and broad light absorption, extending to even the NIR region (**Fig. 3B-c,d,e**). These indicate the full sunlight absorption of these samples after H_2 treatment, which is in agreement with the colour change from pink to dark green (Pt-WO_3/TiO_2 and Pt-WO_3/TiO_2-Au), and from yellow to black (hollow H:Pt-WO_3) after hydrogen treatment. It should be noted that the presence of Pt NPs on WO_3 has a significant impact on reduction by hydrogen. Facile reduction and change in colour of WO_3 during H_2 treatment could be a result of the

chemisorption and subsequent dissociation of H_2 molecules on the Pt NP surface to very active hydrogen atoms (*i.e.*, hydrogen spillover). These hydrogen atoms then migrate to the WO_3 particles, reducing them to black WO_{3-x} particles.[37] In contrast, no significant change in colour or in the UV-vis spectra was observed for the samples without Pt, neither before nor after H_2 treatment (see Fig. SI-3 for details).

The surface chemical states of Ti and W before and after hydrogen annealing were characterized by X-ray photoelectron spectroscopy (XPS). **Figure 3C** shows the Ti $2p_{3/2}$ XPS spectra of these samples. The Ti $2p_{3/2}$ XPS spectrum of the sample before H_2 treatment shows two peaks at the binding energies of 458.4 eV and 464.1 eV, which are characteristic of Ti^{4+} in anatase TiO_2. The similarities between the obtained Ti $2p_{3/2}$ spectra indicate a similar bonding environment after hydrogen treatment.[38, 39] The W 4f XPS spectra of these samples are shown in **Figure 3D.** For the sample before H_2 treatment, only two XPS peaks at 38.4 and 36.3 eV were found, which are characteristic of W^{6+}. However, after H_2 treatment, the sample exhibits different oxidation states for W. Apart from the two main XPS peaks for W^{6+} at 38.4 and 36.3 eV, the appearance of W^{5+} and W^{4+} is unambiguously observed in the H_2-treated sample. As seen in Fig. 3D, the two peaks located at 34.5 and 36.4 eV are assigned to W^{5+}, and the two peaks centred at 32.1 and 33.5 eV are attributed to W^{4+} species; small peaks at 32.0 and 34.2 eV characteristic of W^{3+} were also found. It should be noted that the WO_3 chemical states could be observed in the as-prepared sample due to the presence of Pt NPs on the WO_3. The dissociation of H_2 molecules on Pt NPs to form H atoms (hydrogen-spillover) could reduce W^{6+}, even at mild temperatures.[40, 41] In contrast, no Pt NPs were located on TiO_2; furthermore, TiO_2 requires severe reduction conditions like high pressure and high temperature.[42, 43] Consequently, a high concentration of oxygen vacancies in the WO_{3-x} matrix can be achieved after H_2 treatment; these vacancies act as trapping sites for electron storage in this material (Fig. SI-4). Moreover, the presence of oxygen vacancies is demonstrated by improved visible/NIR absorption, indicating the introduction of impurity states into the forbidden areas of the WO_3 band structure below the conduction band and a corresponding reduction in excitation energy. Solar harvesting, therefore, is significantly improved.[44,45].

The porous structures of the different samples were characterized using N_2 physical adsorption at 77 K. The specific surface area of our hollow double-shell H:Pt-WO_3/TiO_2-Au nanocomposite reaches 220 $m^2\ g^{-1}$, which is much higher than that of conventional porous TiO_2-P25 (50 $m^2.g^{-1}$), WO_3 (8 $m^2.g^{-1}$), and mixed TiO_2-WO_3 (17 $m^2\ g^{-1}$) (**Table SI-1**). As far as we know, this nanocomposite has a higher surface area than any other WO_3/TiO_2 material that has been reported. [46]

The photocatalytic activity of the hollow double-shell H:Pt-WO_3/TiO_2-Au nanospheres was investigated in the photocatalytic decomposition of HCHO under visible light ($\lambda \geq 420$ nm) and in darkness, compared to those of other H_2-treated samples: hollow H:Pt-WO_3/TiO_2, hollow H:Pt-WO_3, and conventional H:Pt-WO_3, prepared from commercial WO_3 under the same catalytic conditions (see **Table SI-1**). As seen in **Figure 4A**, very high catalytic activity for the hollow double-shell H:Pt-WO_3/TiO_2-Au in the decomposition of HCHO was observed both under visible light and in darkness – much higher, in fact, than for other samples. More than 90% of the HCHO was converted after 6 h of reaction under visible light, and up to 80% HCHO conversion was achieved in darkness after 16 h. In addition, for hollow H:Pt-WO_3/TiO_2 and hollow H:Pt-WO_3, only 42 and 36% HCHO conversion, respectively, were obtained after 6 h under visible light, and 39 and 40% conversion, respectively, were obtained after 18 h in the dark. For the conventional H:Pt-WO_3 sample, only 10 and 5% HCHO conversion were achieved under visible light and in the dark, respectively, in the same catalytic conditions.

Figures 4B and C show the CO_2 generation of these samples. The hollow H:Pt-WO_3/TiO_2-Au exhibits CO_2 generation of 110 and 95 µmol under 6 h of visible light illumination and 18 h in darkness, respectively, which are about 10 times higher than that of the conventional H:Pt-WO_3 (10.5 and 9 µmol, respectively) under the same catalytic conditions (**Table SI-1**). The excellent catalytic activity of our hollow double-shell H:Pt-WO_3/TiO_2-Au could be attributed to its high specific surface (S_{BET} = 230 $m^2\ g^{-1}$) compared to that of conventional H:Pt-WO_3/TiO_2 (~16 $m^2\ g^{-1}$) and H:Pt-WO_3 (~8 $m^2\ g^{-1}$), as well as the unique presence of Au NPs in the sample. In addition, the high surface interface between WO_3 and TiO_2 of the hollow double-shell spheres leads to an improved electron–hole charge separation, which enhances photocatalytic activity. Moreover, the H_2 treatment of the hollow double-shell spheres also has a strong impact on the catalytic performance in darkness, due to the high electron storage capacity of this sample.

On the basis of the observed photocatalytic activities, the quantum efficiency (QE) of the prepared photocatalysts for CO_2 generation under visible light and in darkness was calculated using the following equation: $QE = N_{\text{consumed photons for } CO2}/N_{\text{incident photons}}$; where $N_{\text{absorbed photons}}$ is the number of photons consumed for CO_2 generation and $N_{\text{incident photons}}$ is the total number of incident photons. The details of this calculation are described in the literature.[47-50] The QE for CO_2 generation by our hollow double-shell H:Pt-WO_3/TiO_2-Au is about 77.6% under visible light and in darkness. This QE is much higher than that of conventional H:Pt-WO_3 (7.7%).

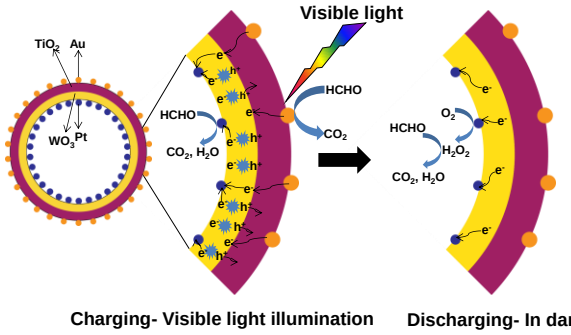

Figure 5. Schematic illustration of the catalytic mechanism of the hollow double-shell H:Pt-WO_3/TiO_2-Au photocatalyst under visible light irradiation and in darkness.

As seen in **Figure 4 and Table SI-1**, in the presence of Pt, all the H_2-treated samples show high CO_2 generation, in the following order: hollow H:Pt-WO_3/TiO_2-Au > hollow H:Pt-WO_3/TiO_2 > hollow H:Pt-WO_3 > conventional H:Pt-WO_3/TiO_2 > conventional H:Pt-WO_3. It is notable that, for the samples without Pt (hollow H:WO_3/TiO_2-Au, hollow H:WO_3/TiO_2, and conventional H:WO_3), no significant CO_2 generation was observed under visible light or in darkness (**Table SI-1**). Thus, the presence of Pt on WO_3 promotes the multielectron reduction of O_2 from the WO_3 conduction band despite the insufficient reduction potential of the conduction band electrons in WO_3 ($O_2 + e^- = O_2^-$ (aq), -0.284 V vs NHE; $O_2 + H^+ + e^- = HO_2$ (aq), -0.046 V vs NHE; +0.5 V vs NHE for WO_3 conduction band).[51] Moreover, it has been demonstrated that the $^{\cdot}OH$ radical is produced by photogenerated electrons on Pt/WO_3, rather than by photogerated holes.[52].

It is noteworthy that this same trend is also observed in the catalytic activity of the samples without hydrogen treatment. However, their catalytic activities are much lower than those of the H_2-treated ones both under visible light and in darkness, as shown in **Figure SI-5** and **Table SI-1.** It is notable that, for the hollow sample in the presence of Au, even before H_2 treatment (*e.g.*, Pt-WO_3/TiO_2-Au), the CO_2 generation rates of this sample under visible light and in darkness are much higher than those of the other samples without Au NPs. This also confirms the significant impact of Au NPs for visible light absorption on TiO_2 surface for photocatalytic performance.

The stability of the hollow H:Pt-WO_3/TiO_2-Au nanocomposite was also studied by performing multi-recycling experiments under the same conditions. As shown in **Fig. SI-6**, after five cycles (*i.e.*, 5 d of reaction), no significant change in activity was observed, indicating the high stability of our hollow photocatalyst in the decomposition of organic pollutants. As shown in **Fig. SI-7A**, the morphology of the as-prepared sample was retained after five cycles. Also, no change in XRD patterns **(Fig. SI-7B)** could be observed for the recycled samples. These results reveal that effective sunlight absorption and high charge carrier separation are required for efficient visible-light-driven photocatalysts. Also, catalytic activity in the dark depends on a number of oxygen vacancies in the WO_{3-x} matrix (**Fig. SI 4**), which can store electrons under light irradiation and discharge them in darkness via Pt NPs (as active sites) for degradation of organic pollutants.[8] Therefore, the excellent catalytic activity of our hollow double-shell H:Pt-WO_3/TiO_2-Au nanospheres under visible light and in darkness could be associated with four main factors: Pt on WO_{3-x}, high interfacial contact between WO_{3-x} and TiO_2 and specific surface area, SPR induced by Au NPs in TiO_2, and oxygen vacancies in the WO_{3-x} matrix.[43]

On the basis of these results, we propose a possible mechanism to explain the excellent photoactivity of our hollow double-shell photocomposite, as described in **Figure 5** and **Figure SI-8.** Our hollow H:Pt-WO_3/TiO_2-Au exhibits excellent performance in the degradation of HCHO. This is due to the synergetic impact of several factors. Under visible light illumination, Au NPs can harvest visible light through SPR to produce "hot" electrons at their surfaces. At the same time, electrons can be produced in the WO_{3-x} conduction band through band gap excitation. Because of suitable energy levels, the "hot" electrons are injected into the TiO_2 conduction band and then into the WO_{3-x} matrix. The photogenerated electrons can be stored in the trapping sites induced by the large amount of oxygen vacancies and simultaneously transferred to the Pt NPs for chemical reactions. In the dark, stored electrons are released and attracted by Pt NPs for the decomposition of organic compounds (**Figs. 5 and SI-8**).

Conclusion

In summary, we have successfully prepared a new type of hollow double-shell H:Pt-WO_3/TiO_2-Au nanosphere using carbon colloidal spheres as the sacrificial template. The obtained photocatalyst showed excellent catalytic activity for the decomposition of HCHO under visible light and in darkness. The enhancement in catalytic activity of this new type of hollow double-shell photocatalyst can be associated with the synergic contributions of Pt NPs as a co-catalyst, the high surface area and TiO_2/WO_3 interfacial contact, plasmonic resonance effects induced by Au NPs, and a large number of oxygen vacancies in the WO_{3-x} matrix. This type of hollow material was reasonably stable under catalytic conditions, and hence, has real potential for air/water degradation both under visible-light illumination and in darkness. Work is in progress to gain further insight into the mechanistic aspects of this process. Furthermore, this strategy can be extended to other hollow double-shell nanocomposite systems for various applications.

Experimental Section

Details about chemicals, synthesis of materials, characterization methods, and photocatalytic test are available in the electronic supporting information (ESI)

Acknowledgements

This work was supported by the Natural Science and Engineering Research Council of Canada (NSERC) through the

Collaborative Research and Development with EXP Inc. (CRD) and Discovery Grants.

Notes and references

1. A. Fujishima and K. Honda, *Nature*, 1972, **238**, 37-38.
2. M. Wang, J. Ioccozia, L. Sun, C. Lin and Z. Lin, *Energy & Environmental Science*, 2014, **7**, 2182-2202.
3. F. Fresno, R. Portela, S. Suárez and J. M. Coronado, *Journal of Materials Chemistry A*, 2014, **2**, 2863-2884.
4. H. Wang, L. Zhang, Z. Chen, J. Hu, S. Li, Z. Wang, J. Liu and X. Wang, *Chemical Society Reviews*, 2014, **43**, 5234-5244.
5. M. R. Gholipour, C.-T. Dinh, F. Béland and T.-O. Do, *Nanoscale*, 2015, **7**, 8187-8208.
6. D. Su, J. Wang, Y. Tang, C. Liu, L. Liu and X. Han, *Chem. Commun.*, 2011, **47**, 4231-4233.
7. T. Tatsuma, S. Saitoh, Y. Ohko and A. Fujishima, *Chemistry of materials*, 2001, **13**, 2838-2842.
8. T. Tatsuma, S. Saitoh, P. Ngaotrakanwiwat, Y. Ohko and A. Fujishima, *Langmuir*, 2002, **18**, 7777-7779.
9. P. Ngaotrakanwiwat, T. Tatsuma, S. Saitoh, Y. Ohko and A. Fujishima, *Physical Chemistry Chemical Physics*, 2003, **5**, 3234-3237.
10. T. Tatsuma, S. Takeda, S. Saitoh, Y. Ohko and A. Fujishima, *Electrochemistry Communications*, 2003, **5**, 793-796.
11. S. Bai, J. Jiang, Q. Zhang and Y. Xiong, *Chemical Society Reviews*, 2015, **44**, 2893-2939.
12. S. K. Dutta, S. K. Mehetor and N. Pradhan, *The Journal of Physical Chemistry Letters*, 2015, **6**, 936-944.
13. P. Christopher, H. Xin and S. Linic, *Nature chemistry*, 2011, **3**, 467-472.
14. S. Linic, U. Aslam, C. Boerigter and M. Morabito, *Nat Mater*, 2015, **14**, 567-576.
15. J. Y. Park, L. R. Baker and G. A. Somorjai, *Chemical reviews*, 2015, **115**, 2781-2817.
16. S. Sarina, E. R. Waclawik and H. Zhu, *Green Chemistry*, 2013, **15**, 1814-1833.
17. X. Sun, Y. Guo, C. Wu and Y. Xie, *Advanced Materials*, 2015, **27**, 3850-3867.
18. S. Wang, H. Qian, Y. Hu, W. Dai, Y. Zhong, J. Chen and X. Hu, *Dalton Transactions*, 2013, **42**, 1122-1128.
19. Y. Liu, L. Yu, Y. Hu, C. Guo, F. Zhang and X. Wen Lou, *Nanoscale*, 2012, **4**, 183-187.
20. C. C. Nguyen, N. N. Vu and T.-O. Do, *Journal of Materials Chemistry A*, 2015, **3**, 18345-18359.
21. C.-T. Dinh, M.-H. Pham, Y. Seo, F. Kleitz and T.-O. Do, *Nanoscale*, 2014, **6**, 4819-4829.
22. M.-H. Pham, C.-T. Dinh, G.-T. Vuong, N.-D. Ta and T.-O. Do, *Physical Chemistry Chemical Physics*, 2014, **16**, 5937-5941.
23. C.-T. Dinh, Y. Seo, T.-D. Nguyen, F. Kleitz and T.-O. Do, *Angewandte Chemie International Edition*, 2012, **51**, 6608-6612.
24. X. Sun and Y. Li, *Angewandte Chemie International Edition*, 2004, **43**, 3827-3831.
25. X. Sun and Y. Li, *Angewandte Chemie International Edition*, 2004, **43**, 597-601.
26. J. B. Joo, Q. Zhang, I. Lee, M. Dahl, F. Zaera and Y. Yin, *Advanced Functional Materials*, 2012, **22**, 166-174.
27. H. Li, Z. Bian, J. Zhu, D. Zhang, G. Li, Y. Huo, H. Li and Y. Lu, *Journal of the American Chemical Society*, 2007, **129**, 8406-8407.
28. C.-T. Dinh, H. Yen, F. Kleitz and T.-O. Do, *Angewandte Chemie International Edition*, 2014, **53**, 6618-6623.
29. D. Ding, K. Liu, S. He, C. Gao and Y. Yin, *Nano Letters*, 2014, **14**, 6731-6736.
30. S. J. Moniz, S. A. Shevlin, D. J. Martin, Z.-X. Guo and J. Tang, *Energy & Environmental Science*, 2015, **8**, 731-759.
31. M. P. Casaletto, A. Longo, A. Martorana, A. Prestianni and A. M. Venezia, *Surface and Interface Analysis*, 2006, **38**, 215-218.
32. H. G. Yang, C. H. Sun, S. Z. Qiao, J. Zou, G. Liu, S. C. Smith, H. M. Cheng and G. Q. Lu, *Nature*, 2008, **453**, 638-641.
33. K. B. Narayanan and N. Sakthivel, *Materials Letters*, 2008, **62**, 4588-4590.
34. X.-L. Li, T.-J. Lou, X.-M. Sun and Y.-D. Li, *Inorganic Chemistry*, 2004, **43**, 5442-5449.
35. N. Serpone, D. Lawless and R. Khairutdinov, *The Journal of Physical Chemistry*, 1995, **99**, 16646-16654.
36. L. Cheng, X. Zhang, B. Liu, H. Wang, Y. Li, Y. Huang and Z. Du, *Nanotechnology*, 2005, **16**, 1341.
37. W. C. Conner and J. L. Falconer, *Chemical Reviews*, 1995, **95**, 759-788.
38. J.-Y. Eom, S.-J. Lim, S.-M. Lee, W.-H. Ryu and H.-S. Kwon, *Journal of Materials Chemistry A*, 2015, **3**, 11183-11188.
39. T.-D. Nguyen-Phan, S. Luo, Z. Liu, A. D. Gamalski, J. Tao, W. Xu, E. A. Stach, D. E. Polyansky, S. D. Senanayake and E. Fujita, *Chemistry of Materials*, 2015, **27**, 6282-6296.
40. S. Khoobiar, *The Journal of Physical Chemistry*, 1964, **68**, 411-412.
41. R. Prins, *Chemical Reviews*, 2012, **112**, 2714-2738.
42. X. Yu, B. Kim and Y. K. Kim, *ACS Catalysis*, 2013, **3**, 2479-2486.
43. X. Chen, L. Liu, P. Y. Yu and S. S. Mao, *Science*, 2011, **331**, 746-750.
44. R. Wu, J. Zhang, Y. Shi, D. Liu and B. Zhang, *Journal of the American Chemical Society*, 2015, **137**, 6983-6986.
45. J. Yan, T. Wang, G. Wu, W. Dai, N. Guan, L. Li and J. Gong, *Advanced Materials*, 2015, **27**, 1580-1586.
46. G. Puma, *Chemical Communications*, 2007, 4749-4751.
47. M. Liu, X. Qiu, M. Miyauchi and K. Hashimoto, *Journal of the American Chemical Society*, 2013, **135**, 10064-10072.
48. M. Liu, R. Inde, M. Nishikawa, X. Qiu, D. Atarashi, E. Sakai, Y. Nosaka, K. Hashimoto and M. Miyauchi, *ACS nano*, 2014, **8**, 7229-7238.
49. J. M. Buriak, P. V. Kamat and K. S. Schanze, *ACS applied materials & interfaces*, 2014, **6**, 11815-11816.
50. H. Kisch and D. Bahnemann, *The Journal of Physical Chemistry Letters*, 2015, **6**, 1907-1910.
51. R. Abe, H. Takami, N. Murakami and B. Ohtani, *Journal of the American Chemical Society*, 2008, **130**, 7780-7781.
52. J. Kim, C. W. Lee and W. Choi, *Environmental science & technology*, 2010, **44**, 6849-6854.

Table of Contents entry:

We report the first synthesis of hollow double-shell H:Pt-WO_3/TiO_2-Au nanospheres with very high specific surface area, high TiO_2/WO_3 interface and strong visible light absorption. This type of materials shows high charge separation and electron storage capacity for efficient degradation of organic pollutants both under visible light and in the dark with very high quantum efficiency. This work opens a new route to develop efficient 24 hours-working photocatalysts for various applications.